# Novel Dual CAFs and Cancer Cell Targeting Nano-Drug Delivery System for Anti-Fibrosis Mechanism of Liver Cancer

**Chunjing Guo**
Ocean University of China
**Xiaoya Hou**
Yantai University
**Xue Liu**
Yantai University
**Changgang Sun**
Weifang Traditional Chinese Hospital
**Daquan Chen** ( cdq1981@126.com )
Yantai University https://orcid.org/0000-0002-6796-0204
**Ming Kong**
Ocean University of China

**Research Article**

**Keywords:** Tumor-associated fibroblasts, Deep penetration, Dual targeting, pH/ROS response, Anti-fibrosis mechanism

**Posted Date:** August 31st, 2021

**DOI:** https://doi.org/10.21203/rs.3.rs-842109/v1

# Abstract

This study proposed the construction of a delivery system based on dual targeting cancer-associated fibroblasts (CAFs) and tumor cell for the treatment of liver cancer. (Z-Glycine-Proline)-Hyaluronic Acid-Sulcanidone-Ginger Anone, named as GHSO, was an amphiphilic carrier material with dual pH/ROS sensitive and dual targeting properties that could be used to load hydrophobic drug to improve their solubility and enhance biocompatibility. Consequently, we combined paclitaxel (PTX) with GHSO to design a novel nano-micelles, called GHSO@PTX micelles. Also, we prepared a single targeted nano-micelles (Hyaluronic Acid-Sulcanidone-Ginger Anone) named HSO@PTX. The GHSO@PTX micelles was 159.40±14.30 nm-sized in neutral water. The electron microscopy results showed that the two micelles were relatively uniform in size and spherical in shape. The results of in vitro release experiments shown that GHSO@PTX micelles had better pH sensitivity and ROS responsiveness. Under the conditions of low pH/high $H_2O_2$ concentration, the cumulative release of micelles was the largest, which could achieve better therapeutic effects. Cell uptake, cytotoxicity of GHSO@PTX micelles were examined at different concentrations by using SMMC-7721 cells and CAFs. The 3D tumor ball experiment showed that GHSO@Cur micelles were more permeable than HSO@Cur, and proved the superiority of GHSO carrier. It first targeted CAFs cells, opened the physical barrier of tumor cells, and achieved deep penetration of tumor sites. We conducted pathological studies and immunohistochemical studies on isolated tissues and tumor tissue sections of nude mice, and investigated the safety and effectiveness of the preparations H&E staining confirmed its safety, Ki 67 was down-regulated, proving that tumor cell proliferation was inhibited, and the down-regulation of α-SMA and Masson proved that CAFs were inhibited and the preparation GHSO@PTX has the effect of killing CAFs and reducing the fibrosis of the tumor. A promising hyaluronic acid-based nanomedicine platform acts as a new drug delivery system to enhance the deep penetration effect of the tumor, and reduce the degree of fibrosis.


# 1. Introduction

Despite the rapid development of new treatments, the malignant tumor remains one of the significant causes of human death worldwide. Currently, most clinical treatments are targeting tumor cells, ignoring the surrounding tumor microenvironment (tumor microenvironment, TME). The TME includes all physiological and biochemical elements, primarily including the extracellular matrix (extracellular matrix, ECM), tumor-related fibroblast (cancer-associated fibroblasts, CAFs), tumor-related immune cells, tumor vascular systems, and low oxygen and acidic environment[1]. Solid tumors, especially pancreatic cancer, bladder cancer, and breast cancer are all composed of rich CAFs and excess ECM, creating a physical barrier that prevents the transmission of tumor-centric treatment to tumor cells[2–4]. The main treatments currently are surgical resection, radiotherapy, ablation, and interventional therapy, which may also kill some of the pericancerous tissue, but they are difficult to inhibit tumor recurrence from the root.

More and more research demonstrated that fibrous TME played an important role in accelerating tumor progression and deterioration. Since the rare lethal tumor cells "seeds" are cultivated and protected by the rich tumor matrix "soil", targeted nano-drug therapy based on these complex features of cancer cells

cannot fully control the pathological processes of cancer development by TME. Moreover, after passing through the tumor blood vessels, the nano-drugs targeted by dense ECM, cancer cells are often retained in the tumor matrix and unable to penetrate inside the tumor, resulting in an insufficient concentration of local drug in the deep tumor to inhibit the deteriorating[5, 6]of the tumor cells located in the deep part. Therefore, exerting appropriate TME remodeling, reversing the tumor promoting role and improving deep drug penetration was key to effectively improving cancer nanotreatment.

Epidemiological and clinical studies have shown that tissue fibrosis in certain organs such as the liver and pancreas is a precursor to corresponding cancer[7–9]. For example, stationary pancreatic and hepatic star cells can obtain CAFs-like phenotypes in pancreatic and liver cancer. CAFs, as a network cell, are steady with little antigen misfortune and treatment obstruction; enormous aggregate contrasts of tumor cells between people, while grid cells are non-harmful cells with somewhat single phenotype[10–12]. The fibroblast activated protein (FAP) is one of the most important molecular markers on the CAFs surface, which became a potential target for tumor immunotherapy[13–15]. FAP is a type II complete membrane serine protease overexpressed by CAFs, selectively expressed in over 90% of human epithelial tumors, and is considered a generic tumor antigen and a promising target for CAFs depletion[16, 17]. Z-glycine-proline (ZGP) is a small molecule peptide that can specifically target FAP[18–20].

Natural polysaccharides, with the attributes of good biocompatibility, degradability, easily soluble in water, low toxicity, and easy modification, have been more and more favored by researchers and widely used in the research of nano-drug delivery system[21–23]. As of now broadly utilized are hyaluronic corrosive (hyaluronic corrosive, HA), (chitosan, CS), Columbus polysaccharide, lentinan polysaccharide, angelica polysaccharide, and so forth[24–27]. Natural polysaccharides as a drug carrier, can not only improve the stability of drugs, reduce the toxic side effects of drugs, avoid accumulation and residue in normal tissues, but also has some biological characteristics, such as antioxidant, adjust the body's immune functions[28, 29]. The CD44 receptor is an adhesion receptor present on the surface of most tumor cells, and is also highly expressed on macrophages and fibroblasts at inflammatory sites in the meantime[30–32]. HA can be explicitly adsorbed with CD44 receptors as target particles for CD44 receptors, and hence HA is broadly utilized in the development of nanocarriers[33–35].

The endogenous stimulation response generally utilizes the physiological environment from normal tissue cells, achieving the purpose of drug release through chemical reactions, commonly including pH, reactive oxygen clusters, high concentration of glutathione (GSH), enzymes, glucose, magnetic field, light, and so on[36–41]. This response is sensitive and accurate in drug release, can accelerate cellular release, improve cellular toxicity, and multidrug resistance[42]containing drug nanoparticles. Two main carrier materials are using pH-sensitive design, one in the form of predrug, namely, the drug is directly connected to the acid-sensitive bond, and the drug is disconnected in the acid environment of low pH; the other is to de-load the drug through the acid-sensitive carrier and in the acid-sensitive environment. Common acid-sensitive bonds are oxime, acetaldehyde, imines and vinyl ether[43, 44]. Activated oxygen (reactive oxygen species, ROS) is a class of reactive substances that produce within cells and participate in many molecular biological processes, including $H_2O_2$,$OCl^-$•OH and $O^{2-}$. Under normal physiological conditions,

the low concentration of ROS is involved in many metabolic pathways as signaling molecules, when they are beneficial to the body. It was found that an oxidative stress response occurs if a large amount of ROS, is produced in the cells, leading to the occurrence of various diseases. In the early stage of inflammation, excess ROS can not only oxidate lipoprotein but also induce apoptosis and accelerate the progression of the inflammatory site[45]. Due to the metastasis of cancer cells, it can be used as a special stimulatory factor for drug release. Many ROS responsive agents have been explored using high active ROS vectors. It mainly includes sulfur-containing polymer ROS response carrier, selenium-containing ROS response carrier, and tellurium-containing polymer ROS response carrier, such as borate, polysulfide, ferrocene, anthocyanins, etc[46–48].

Herein, given the current disadvantages of tumor treatment, this paper focused on the tumor itself and its surrounding microenvironment, designs a dual-pronged targeted treatment mode, and hoped to achieve a better tumor treatment effect. First, hyaluronic acid (HA) that targets the CD44 receptor on the tumor cell surface was selected as the main backbone of the biophilic vector material and introducing z-glycine-proline (ZGP) on its surface can specifically target the FAP receptor on the CAFs surface, achieving the purpose of double targeting tumor cells and CAFs. Then, sensitive groups (thiones and acetones) responding to high ROS and low pH in tumor cells were introduced to achieve drug release in tumor cells, reducing damage to other non-tumor cells. The nanomicelles as the drug delivery system improved the solubility of PTX and the stability of the drug. When the nanomicelles GHSO@PTX reached the tumor site, it first made contact with the matrix cells around the tumor cells, killing it by the endocytic release drug through specific binding to CAFs. CAFs were killed, both opened the barrier and reduced TGF-β secretion, reducing the promoting effect on tumor cells and reduce the degree of fibrosis. The whole mechanism(Fig. 1) realized a targeted treatment strategy of killing tumor cells and inhibiting tumor-promoting microenvironment.

## 2. Materials And Methods

# 2.1 Chemicals, Cell lines and Animals

Zingiberone,ZGP and PTX were obtained from Aladdin Chemistry Co., Ltd. TKL was received from Shanghai Chuangyan Chemical Technology Co., Ltd. HA was achieved from Huaxi Forida Biotechnology Limited. N-(3-Dlmethylamlnopropyl)-N’-ethylcarbodllmide hydrochloride (EDC), Dimethyl Sulphoxide (DMSO), 4-Dimethylaminopyridine (DMAP), 1-Hydroxybenzotriazole Hydrate (HOBT), Succinimide (NHS) were bought from Tianjin Yongda Chemical Reagents Co., Ltd. $H_2O_2$ was gained from Aladdin reagent net.3-(4,5-dimethylthiazol-2-yl)-2,5-diphenyl tetrazolium bromide (MTT, Sigma-Aldrich, St. Louis, MO), DMEM (High Glucose), and fetal bovine serum (FBS) were purchased from Junshuo Biotech Co., Ltd (Yantai, China).

NIH 3T3 (Normal tissue fibroblasts) was got from BeNa Culture Collection (Beijing, China). The SMMC-7721 cell line (hepatoma carcinoma cell) was obtained from Shandong Academy of Pharmaceutical Science.

The NU/NU female nude mice were procured from Beijing Vital River Laboratory Animal Technology Co. Ltd (SPF grade, 6–8 weeks, 18–22 g). The experimental process was carried out in strict accordance with the relevant regulations of the Committee on the Management and use of Experimental Animals in Yantai University and the National Institute of Health Guide for the Care and Use of Laboratory Animals. Nude mice were divided into six groups with four mice in each group. These groups were: Free PTX group, HSO@PTX(-) group, HSO@PTX(+) group, GHSO@PTX(-) group, and GHSO@PTX(+) group.

## 2.2 Synthesis and characterization of GHSO

In three bottles of 150 mL with thermometer, water distributor, reflux condensate tube, added zingiberone: glycerol: cyclohexane (molar ratio of 1: 1.0 ~ 1.5: 1), added p-toluene sulfonic acid as catalyst, mole ratio of p-toluene sulfonic acid and gingerone was 1: 150 ~ 250, this reaction condensed reflux 6 h at 92 ℃. After removal of toluene after the reaction, ethyl acetate and saturated sodium carbonate were added for washing extraction 3 ~ 4 times and 45 mL/ times, and dried. Purpurified compounds were separated after drying, when the expanant oil ether: ethyl acetate = 1: 1, the products were collected at this proportion and ZO compounds were made.

The formamide (6 mL), ZO (100 mg), TKL (27.86 mg), EDC and DMAP were added into the 50 mL round bottom flask and magnetically stirred until they were completely dissolved at room temperature. After stirring the reaction at room temperature for half an hour, the reaction temperature was gradually raised to 40℃ in an oil bath. After 24 h the product ginger azone-thiazone (so) was obtained. Further, 150 mg of HA was added into the reaction system, and the crude product was continuously reacted for 48 hours.The crude product was dialyzed by using a dialysis bag (2000 Da MWCO). HA-SS-SO(HSO) was obtained of continuous drying using a freeze dryer. Finally, The formamide (7 mL), HSO (92.6 mg), ZGP (20 mg), EDC and NHS were added into the round bottom flask and magnetically stirred until they were completely dissolved. After a reaction of 24 h, at 30℃, they were transferred to the molecular weight dialysis bag of 2000 Da in accordance with the above dialysis method and freeze-dried to obtain the final carrier material GHSO. The synthetic route of this reaction is shown in Fig. 2.

$^{1}$ H-NMR spectroscopy was used to detect the chemical structure of GHSO. A total of 10 mg of GHSO was weighed and dissolved in 0.6 mL of $D_2O$ and $d_6$-DMSO to detect the chemical shifts.

## 2.3 Preparation of the GHSO@PTX nanomicelles

The synthetic GHSO can load PTX by self-assembly. GHSO (10 mg) and PTX (1 mg) dissolved in formamide were added into the dialysis bag (2000 Da). The dialysis water was replaced almost every 2 hours till the formamide in the dialysis bag was completely gone. Thereafter, we obtained the nanomicelles of GHSO@PTX. IR spectra for GHSO materials were tested and determined at room temperature.

## 2.4 Characterization of the GHSO@PTX nanomicelles

The HSO@PTX and GHSO@PTX micelles obtained by the above preparation method were determined by the particle size, PDI, potential. The nanomicelles HSO@PTX and GHSO@PTX, obtained by the above

preparation method were repeatedly dropped on the copper network, naturally dried with phosphotungstic acid, and the morphology of the nanogels was observed with a transmission radio microscope. The Encapsulation efficiency (EE%) and Drug loading (DL%) capacity of nanomicelles HSO@PTX and GHSO@PTX were determined by HPLC.

EE(%) = (Weight of Cur in HASF@Cur micelles)/(The weight of all added Cur)× 100%

DL(%) = (Mass of Cur in HASF@Cur micelles)/(Total Mass of the HASF@Cur micelles) × 100%

# 2.5 Experimental study on in vitro release of the GHSO@PTX nanomicelles

To examine the responsive release characteristic of PTX from GHSO@PTX, the release profiles were examined by using dialysis method. First, we examined the ROS-responsive PTX release capacity of the GHSO@PTX. Briefly, 1 mL GHSO@PTX was placed in a dialysis bag (MWCO 2000 Da) and immersed in 50 mL PBS buffer containing 0.5% (v:v) Tween 80 with different $H_2O_2$ and pH concentrations (pH 7.4, $H_2O_2$ 0.1 mM; pH 7.4, $H_2O_2$ 1 mM; pH 7.4, $H_2O_2$ 10 mM; pH 5.8, $H_2O_2$ 0.1 mM; pH 5.8, $H_2O_2$ 1 mM; pH 5.8, $H_2O_2$ 10 mM). The whole system was agitated at 37°C and sampled at pre-defined time points. The sample solution was taken from different time points and different release media, after the filter film exceeded 0.22 μm, the concentration content of PTX was determined with the high-performance liquid phase and the cumulative release amount under different release media.

# 2.6 Cytotoxicity assessment

To investigate the safety of the blank carrier material, the SMMC-7721 cells or CAFs were co-incubated with blank GHSO of various doses (10–500 μg/mL) at 37°C. 20 μL of MTT (5 mg/mL) was added to the per well. After 4 h, the supernatant medium was taken the place of DMSO (200 μL) and shaken for 10 min. The microplate reader (Thermo Fisher Scientific Co., Waltham, MA) was used to determine the absorbance.

The effects of PTX preparations on SMMC-7721 cells and CAFs in vitro were examined by using an MTT assay. To compare the viability effects, Free PTX, HSO@PTX, and GHSO@PTX were fully dissolved in DMEM for final PTX concentrations from 1.25 μg/mL to 40 μg/mL. Typically, after counting, SMMC-7721 cells or CAFs cells were uniformly dispersed in cell culture medium at a density of 10,000 cells/mL, and 200 μL of the cell suspension was placed in each well of a 96-well plate, and cultured overnight until the cells were fully adherence. Subsequently, fresh DMEM-containing PTX preparations were replaced and incubated for an additional 24 or 48 h. The microplate reader was conducted to gauge the relative cell viability. We could calculate cell survival (%) according to the following formula:

Cell survival%=$A_T$-$A_0$/$A_C$-$A_0$×100%

# 2.7 Cellular uptake

The fresh medium containing Free PTX, HSO@PTX micelles, or GHSO@PTX micelles were added to replace the original medium after 24 h (48 h), respectively. The SMMC-7721 cells or CAFs were then cultured for 0.5 h, 1 h, 2 h, and 4 h (PTX concentration: 20 μg/mL) or for 4 h with following different concentrations of PpTX : 5 μg/mL, 10 μg/mL, 20 μg/mL, and 40 μg/mL in above atmosphere. The consequence of cellular uptake was observed by inverted fluorescence microscope to have a qualitative analysis.

## 2.8 In vitro penetration of different nanoparticles in tumor cells and fibroblast-mixed multicellular hybrid tumor spheroids

To mimic the solid tumor microenvironment in which tumor cells and fibroblasts grow together, we established CAFs cells & SMMC-7721 cells cocultured hybrid tumor spheroids. The in vitro tumor penetration ability of Cur-labeled nanoparticles with or without ZGP incubation was investigated on hybrid tumor spheroids. The multicellular tumor spheroids were established according to a previous report.28 Briefly, 80 μL of hot 2.0% agarose solution (w/v) was added to 96-well plates and then cooled to room temperature. SMMC-7721 cells were mixed with fibroblasts at a ratio of 2:1, seeded in 96-well plates, and cultured for 2–3 days to grow into a spheroid. Then, HSO@Cur and GHSO@Cur were added for incubation to observe the effect of penetration.

## 2.9 In vivo distribution of mice xenografted

The in vivo distribution was measured by In-Vivo FX Pro in vivo imaging system. To observe the accumulation of PTX, HSO@PTX micelles and GHSO@PTX micelles in vivo, the Free DiR, HSO@DiR and GHSO@DiR micelles (at the DiR concentration at 500 μg/mL) were injected into SMMC-7721 and CAFs tumor-bearing mice via the tail vein. On hour 12 after injection of kinds of DiR, and the tumor and the major organs of mice were collected and the fluorescence intensity of various organs was monitored in vitro by In-Vivo FX Pro.

## 2.10 In vivo pharmacodynamics study

Docking nude mice were randomly divided into 6 groups, 3 in each group, raised separately and marked, and began to give the medicine when the tumor grew to the appropriate volume. The administration group was Saline, Free PTX, HSO@PTX(-), HSO@PTX(+), GHSO@PTX(-), GHSO@PTX(+), with high and low concentrations of the high concentration. The tumor grew up to 100 $mm^3$ for tail IV administration (5 mg/Kg), administered every 3 days. Each administered, weight and tumor volume were measured for a period of 30 days. Three days after the administration, all the naked rats were euthanized, and the heart, liver, spleen, lung, kidney and tumor tissue were dissected and stored in 4% polyformaldehyde respectively. The weight change curve, volume change and tumor suppression rate of each group were drawn according to the experimental records. The specific formula is as follows:

$$V = \frac{1}{2\ (L \times W^2)}$$

$$TIR = \frac{W_{control} - W_{tested}}{W_{control}} \times 100\%$$

Where *L* and *W* are the length and width of the tumor, respectively; $W_{control}$ is the tumor weight of the control group and $W_{tested}$ is the tumor weight of the experimental group.

### 2.11 Preliminary histological study

Remove the isolated tissue previously fixed to polyformaldehyde, bury paraffin, and dry in a 60 ℃ oven after slicing. After that, the isolated organ tissue sections and tumor tissue of different drug administration groups were stained by H&E, sealed after dyeing the volatile xylene, observed under the microscope, and took photos.

### 2.12 Immunohistochemistry

To evaluate the growth inhibition of the tumor cells, the expression of Ki 67 in the tumor cells was investigated. To verify the inhibitory effect of GHSO@PTX on the tumor microenvironment and antifibrosis, α-SMA and Masson staining were performed, and the number of α-SMA-positive cells and collagen content in the tumor tissues were examined.

### 2.13 Statistical analyses

All data are performed with Student's t-test and ANOVA. The quantitative data were presented as mean ± standard deviation (SD).

## 3. Results And Discussions

3.1 Characterization of GHSO materials

$^1$H-NMR

The $^1$H-NMR spectroscopy of HA, HSO and GHSO were clearly emerged in Figure 3. The methyl peak for TKL was observed at about δ: 1.5. $^1$H-NMR spectra revealed absorption peak at about δ: 4.77, which was -OH in ZO. The appearance of the signal peak at δ: 7.1 verified the presence of ZGP, indicating that the new product of GHSO had been synthesized successfully.

FT-IR

FT-IR spectra of GHSO materials were shown in Figure 4. A referred to together dimethyl group, coupled to split into two special shape spectral bands near 1375cm$^{-1}$, The double-peak in the picture testified the connection of the TKL. B, C referred to skeleton vibration peak of the aromatic ring, D referred to vibration coupling peak of ZO, 1083 cm$^{-1}$.

3.2 Particle Size, Zeta Potential, Morphology, EE% and DL%

The results of Figure 5 showed that the particle size of HSO@PTX micelles was 143.30±17.00 nm, the PDI was 0.236±0.004, the potential was -23.76±5.12 mV, the encapsulation efficiency (EE%) was 46.47±2.80%, and the drug loading (DL%) was 4.57±0.68%. The particle size of GHSO@PTX micelles was 159.40±14.30 nm, PDI was 0.159±0.06, potential was -24.99±4.73 mV, EE% was 49.61±3.52% and DL% was 4.72±0.39%. The electron microscopy results shown that the two micelles were relatively uniform in size and spherical in shape.

3.3 Drug release investigation

GHSO@PTX at different H2O2 concentrations and pH conditions are shown in Figure 6 below. It can be seen from the figure that each group was slowly released under the conditions and had no sudden release. For the first three groups, the control variable pH remained unchanged at 7.4. As we can see that the H2O2 concentration increased from 0.1 mM to 1 mM, to 10 mM, which was 31%, 38%, and 34% respectively. See that when the H2O2 concentration, the cumulative release increased significantly at 10 mM, for fracture of affinity vector material GHSO under high concentration H2O2, promoting drug release. When the H2O2 concentration was constant and all 10 mM, it showed obvious growth in pH 5.8(76%) compared with pH 7.4(54%), which proved a promoting effect of low pH on nanomicelles. The analysis reason was pH 5.8, ginger acetone bond fracture of GHSO, the conformational change of two affinity carrier materials, micelles dissociation, and promote drug release.

3.4 Cytotoxicity assessment

The cytotoxicity results of nanomicelles to SMMC-7721 cells and CAFs were shown in Figure 7. Figure 7 (E) represented the growth inhibition of blank micelles on both cells at 24 h. It was obvious from the figure that the toxicity of blank micelles is very small, with the survival of 500% at the concentration of 500 μg/ml, demonstrating that the in vivo safety of our designed affinity vector material GHSO was good.

In Figure 7, Figure 7 (A) and (B) represented cytotoxicity results on SMMC-7721 cells by different administration groups at 24 h and 48 h, respectively. Meanwhile, Figure 7 (C) and (D) represented cytotoxicity results on CAFs cells by different administration groups at 24 h and 48 h, respectively. The results showed that with the increase of drug concentration, the survival rate of each drug group decreased to different degrees. At the same drug concentration, the cell survival of nanomicelles group was lower than that of Free PTX, indicating that the nanomicelles group had a stronger lethal effect on tumor cells, probably because HA played the main role in the targeting of tumor cells SMMC-7721. In

Figure 7 (C) and (D), the GHSO@PTX group showed the strongest cytotoxicity, possibly due to the fact that it could target CAFs, to enhance the therapeutic effect of tumors.

3.5 Cellular uptake

Figure 8 represented the uptake effect of Free Cur, HSO@Cur, GHSO@Cur on SMMC-7721 cells (A) and CAFs cells (B) at different times. The results in the figure showed that the intake of both cells in each administration group has increased over time. In Figure 8 (A), the nanomicelles group uptake effect was much better than in the Free drug group. In Figure 8 (B), tthe uptake effect of the nanomicelles bunch was superior to the Free medication bunch simultaneously, and the take-up impact of the nanomicelles GHSO@Cur bunch was ideal, additionally in view of its designated impact on CAFs.

Figure 8 (C) and (D) represented the uptake effect at different drug concentrations. It could be seen from the figure that, as the drug concentration increases, the intake effect of each drug administration group has increased to varying degrees. In Figure 8 (C), the uptake of HSO@Cur and GHSO@Cur were better compared with the Free Cur group, proving the superiority of nanomicelles. Another reason was that HA could target the CD44 receptor on the surface of tumor cells, but the two nanomicelles were not significantly different because ZGP was specific for targeting FAPα enzyme on CAFs cell surface and does not promote the uptake of tumor cells. In Figure 8 (D), the nanomicelles group was also better than the free drug group, but the GHSO@Cur group was significantly stronger than the HSO@Cur group because GHSO is specific for targeting CAFs, and thus more uptake superiority, consistent with the initial scenario.

3.6 In vitro penetration of multicellular hybrid tumor spheroids

In this experiment, Cur was selected as a fluorescent substance, loaded in the two affinity vector materials HSO and GHSO, to investigate the in vitro tumor ball penetration effect of two nanomicelles. Figure 9 (A) represented the GHSO@Cur group, Figure 9 (B) represented the HSO@Cur group, and the middle black site represented the site where the nanomicelles failed to reach. It was obvious that in the 3D tumor ball of different particle size, the deep penetration effect of the GHSO@Cur group was significantly stronger than that of the HSO@Cur group. For the analysis reason, it might be that the double-targeted nanomicelles GHSO@Cur group could first target the CAFs, to open the barrier and better achieve the deep penetration of the nanomicelles.

3.7 In vivo fluorescence imaging

The results in Figure 10 shown that the HSO@DiR and GHSO@DiR groups compared with the control Free DiR solution group, DiR can be better delivered to the tumor tissue at about 8 h and accumulate more to the tumor tissue site over time. It was worth noting that the GHSO@DiR group reached the tumor tissue one step earlier than the HSO@DiR group and had a stronger fluorescence intensity at the tumor. At the early stage of administration, the nanomicelles group were distributed at the main organs. Over time, the

impact on the main organs had decreased a lot. By 24 h, the double-targeted GHSO@DiR group had the least impact on the main organs, but had the most savings in the tumor site.

The figure on the right represents the results of fluorescence imaging of isolated tissue and organs after administration of 12 h. The results showed that there was no accumulation of the tumor site in the control Free DiR solution group, and both groups of nanomicelles could deliver DiR to the tumor site, demonstrating the superiority of the nanodrug delivery system, and the targeting of HA to tumor cells achieved DiR delivery in the HSO@DiR group. The dual-targeted GHSO@DiR group had the most savings in the tumor site, possibly due to the ZGP targeting of CAFs promoting nanopelels into the tumor tissue. The accumulation of three groups of organs was mainly liver and spleen, the analysis reason might be because the liver as an important metabolic organ of the body, these foreign substances were metabolized by the liver, leading to the accumulation in the liver site; or because preparations are swallowed by macrophages in the body's mesh endothelial cell system, with more macrophages in the liver and spleen, leading in the most accumulation of the liver and spleen parts.

3.8 In vivo pharmacodynamics study

Both Figure10 (A) and 10 (C) could intuitively observe that the HSO@PTX and GHSO@PTX groups are significantly better than the free drug PTX groups, possibly because the nanodrug delivery system could better deliver the drug to the tumor site, improve the effective content of the drug in the tumor site, and play a good therapeutic role, demonstrating the characteristics of pH sensitivity and ROS response. GHSO@PTX group compared with the HSO@PTX group, the treatment effect was better, the analysis might be because GHSO@PTX could specifically target the matrix CAFs, around tumor cells for nanoparticles removal obstacles, promote nanoparticles to better achieve deeper penetration of tumors. The treatment effect of high concentration of GHSO@PTX(+) group was higher than that of GHSO@PTX(-), and there was no naked rat death caused by high concentration during administration, which also affirmed the good compatibility of the carrier material, improved the treatment concentration of the drug and reduced the toxic side effects of the drug. As can be seen from Figure10 (D), the weight of naked rats in the nanopelel group did not change significantly in the early administration, and showed a slight decrease in the later administration, which proved that the nanopelels were less toxic and have certain safety in the body.

3.9 Preliminary histological study

It could be seen from Figure 12 that HSO@PTX and GHSO@PTX had very small damage to the heart, liver, spleen, lung, and kidney of naked rats, combined with the weight change of naked rats, but also more proved the safety of the two affinity carrier materials, reduced the toxicity of drugs, and played a good transport role. It could be seen from the H&E staining results of the tumor tissue of nude tumor rats, there was no damage in the tumor tissue of the saline group, which as a control, observed the free drug group and no excessive damage to the tumor tissue. The analysis might be that the free drug PTX failed to reach the tumor tissue too much and did not play an effective therapeutic effect. Observe the nanosheel group, we found obvious damage to tumor tissue and large death of tumor cells, which proved

the inhibitory effect of nanosheel on tumor cells, especially the high concentration GHSO@PTX(+) group, the most loose distribution and obvious core consolidation shrinkage, and proved the best treatment effect of double-targeted nanosheel high concentration GHSO@PTX(+) group.

3.10 Immunohistochemistry

Ki 67 is an important marker of cell proliferative activity. High-level expression of Ki 67 represents a strong cell proliferative activity and can be used as a reliable evaluation indicator after tumor treatment. The results showed that the expression of Ki 67 in the high concentration of GHSO@PTX(+) group was significantly reduced, proving that the tumor cell proliferation activity was significantly inhibited, and that the double-targeted nanogelam GHSO@PTX had a good role in tumor therapy. CAFs cells are α-SMA positive cells, α-SMA staining can brown α-SMA positive cells, and we can judge using the number of brown cells. It can be seen from the figure that, compared with the saline group and the free drug group, the significant reduction of brown cells in the GHSO@PTX group was reduced, indicating that the number of CAFs cells was significantly reduced. The reason analysis may be because GHSO can target the FAP α enzyme on the CAFs surface, and then enter CAFs, to realize the lethal effect on CAFs, thus reducing the promoting effect of tumor microenvironment on the growth of tumor cells. Masson tricolor staining is a classic staining method for collagen cellulose, which dyes collagen cellulose blue. Collagen cellulose is secreted by CAFs cells, deposited in microenvironments, leading to liver fibrosis and promoting the development of tumor cells. From the figure, the blue lines of nanolymical group GHSO@PTX were significantly reduced, indicating decreased collagen secretion, also proving that CAFs is inhibited, while decreased collagen deposition, but also indicating inhibiting the development of liver fibrosis.

# 4. Conclusions

- In chemical synthesis, the affinity nano-carrier material HSO, with pH sensitivity and ROS response was synthesized to connect the deep penetration of the target with CAFs targeting function, synthesize the final carrier material GHSO, and conduct a series of characterization of the carrier material to verify the successful synthesis. Nanomicelles were prepared by the carrier load drug PTX, dialysis, and investigated the particle size, potential and electric mirror. In vitro release experiments verified the pH sensitivity and ROS responsiveness of the carrier material. In the cell experiment, the 3D tumor ball deep penetration experiment was studied to investigate the cell penetration of the in vitro tumor ball through multiple cell culture in vitro. In the immunohistochemical experiment, the obvious reduction of Ki 67 meaned that the proliferation activity of tumor cells was suppressed and the decrease of α-SMA-positive cells, which proved the targeting of GHSO@PTX to CAFs, the decrease of collagen fiber content, reduced the degree of tumor tissue fibrosis, and opened up new ideas for anti-fibrosis therapy.

# Declarations

**Acknowledgements**

This study was financially supported by Taishan Scholar Foundation of Shandong Province (No.qnts20161035); Natural Science Foundation of Shandong Province (No.ZR2019ZD24, ZR2019YQ30); Graduate Innovation Foundation of Yantai University, GIFYTU.

### Authors' contributions

CG, XH and XL conceived of this study and designed it. DC contributed to data collection and article writing. CS and MK performed the preparation of the references in the manuscript. All authors read and approved the final manuscript.

### Funding

This funding was supported by Taishan Scholar Foundation of Shandong Province (No.qnts20161035); Natural Science Foundation of Shandong Province (No. ZR2019ZD24,ZR2019YQ30).

### Availability of data and materials

All data generated or analyzed in this study are included in this article.

### Ethics approval and consent to participate

All procedures involving laboratory animals are performed in accordance with the ethics committee guidelines at the Ocean University of China and Yantai University.

### Consent for publication

Not applicable.

### Competing interests

The authors declare no conflict of interest in this article.

## References

1. Chen Q, Liu GX, Liu S, Su HY, Wang Y, Li JY, Luo C. Remodeling the tumor microenvironment with emerging nanotherapeutics. Trends in pharmacological sciences. 2018; 39(1): 59-74.
2. Chang A, Kim-Fuchs C, Le CP, Hollande F, Sloan EK. Neural regulation of pancreatic cancer: a novel target for intervention. Cancers. 2015; 7(3): 1292-1312.
3. Zhang J, Miao L, Guo ST, Zhang Y, Zhang L, Satterlee A, Kim WY, Huang L. Synergistic anti-tumor effects of combined gemcitabine and cisplatin nanoparticles in a stroma-rich bladder carcinoma model. Journal of Controlled Release. 2014; 182: 90-96.
4. Zhang B, Hu Y, Pang ZQ. Modulating the tumor microenvironment to enhance tumor nanomedicine delivery. Frontiers in pharmacology. 2017; 8: 952.

5. Fernandes C, Suares D, Yergeri MC. Tumor microenvironment targeted nanotherapy. Frontiers in pharmacology. 2018; 9: 1230.
6. Chen XM, Song E. Turning foes to friends: targeting cancer-associated fibroblasts. Nature reviews Drug discovery. 2019; 18: 99-115.
7. Jacobetz MA, Chan DS, Neesse A, Bapiro TE, Cook N, Frese KK, Feig C, Nakagawa T, Caldwell ME, Zecchini HI. Hyaluronan impairs vascular function and drug delivery in a mouse model of pancreatic cancer. Gut. 2013; 62(1): 112-120.
8. Wong KM, Horton KJ, Coveler AL, Hingorani SR, Harris WP. Targeting the tumor stroma: the biology and clinical development of pegylated recombinant human hyaluronidase (PEGPH20). Current oncology reports. 2017; 19(7): 47.
9. Ishii G, Ochiai A, Neri S. Phenotypic and functional heterogeneity of cancer-associated fibroblast within the tumor microenvironment. Advanced drug delivery reviews. 2016; 99: 186-196.
10. Guo J, Zeng HT, Chen Y. Emerging nano drug delivery systems targeting cancer-associated fibroblasts for improved antitumor effect and tumor drug penetration. Molecular pharmaceutics. 2020; 17(4): 1028-1048.
11. Truffi M, Mazzucchelli S, Bonizzi A, Sorrentino L, Allevi R, Vanna R, Morasso C, Corsi F, Nano-strategies to target breast cancer-associated fibroblasts: rearranging the tumor microenvironment to achieve antitumor efficacy. International journal of molecular sciences. 2019; 20(6): 1263.
12. Yang M, Li J, Gu P, Fan X. The application of nanoparticles in cancer immunotherapy: Targeting tumor microenvironment. Bioactive materials. 2021; 6(7): 1973-1987.
13. Santos AM, Jung J, Aziz N, Kissil JL, Puré E. Targeting fibroblast activation protein inhibits tumor stromagenesis and growth in mice. The Journal of clinical investigation. 2009; 119(12): 3613-3625.
14. Bhuvaneswari C, Ng QF, Thong PS, Soo KC. Nimotuzumab increases the anti-tumor effect of photodynamic therapy in an oral tumor model. Oncotarget. 2015; 6(15): 13487-13505.
15. Gollnick SO, Brackett CM. Enhancement of anti-tumor immunity by photodynamic therapy. Immunologic research. 2010; 46: 216-226.
16. Fang J, Xiao L, Joo KI, Liu Y, Zhang C, Liu S, Conti PS, Li Z, Wang P. A potent immunotoxin targeting fibroblast activation protein for treatment of breast cancer in mice. International journal of cancer. 2016; 138(4): 1013-1023.
17. Ji TJ, Zhao Y, Ding YP, Wang J, Zhao RF, Lang JY, et al. Transformable peptide nanocarriers for expeditious drug release and effective cancer therapy via cancer-associated fibroblast activation. Angewandte Chemie. 2016; 55(3): 1050-1055.
18. Liu M, Song W, Huang L. Drug delivery systems targeting tumor-associated fibroblasts for cancer immunotherapy. Cancer letters. 2019; 448: 31-39.
19. Chen BL, Dai WB, Mei D, Liu TZ, Li SX, He B, et al. Comprehensively priming the tumor microenvironment by cancer-associated fibroblast-targeted liposomes for combined therapy with cancer cell-targeted chemotherapeutic drug delivery system. Journal of Controlled Release. 2016; 241: 68-80.

20. Wang J, Li Q, Li XJ, Yuan W, Huang S, Cai S, Xu J. A novel FAPα-based Z-Gly-Pro epirubicin prodrug for improving tumor-targeting chemotherapy. European journal of pharmacology. 2017; 815: 166-172.
21. Rehman A, Jafari SM, Tong Q, Riaz T, Assadpour E, Aadil RM, Niazi S, Khan IM, Shehzad Q, Ali A. Drug nanodelivery systems based on natural polysaccharides against different diseases. Advances in Colloid and Interface Science. 2020: 102251.
22. Naveen C, Shastri NR. Polysaccharide nanomicelles as drug carriers, in: Polysaccharide Carriers for Drug Delivery. Elsevier. 2019: 339-363.
23. Zheng Y, Xie QX, Wang H, Hu YJ, Ren B, Li XF. Recent advances in plant polysaccharide-mediated nano drug delivery systems. International Journal of Biological Macromolecules. 2020; 165: 2668-2683.
24. Zhang XY, Zhao MY, Cao N., Qin W, Zhao M, Wu J, Lin DJ. Construction of a tumor microenvironment pH-responsive cleavable PEGylated hyaluronic acid nano-drug delivery system for colorectal cancer treatment. Biomaterials science. 2020; 8(7): 1885-1896.
25. Liu Y, Wu F, Ding Y, Zhu B, Su Y, Zhu X. Preparation and characterization of paclitaxel/chitosan nanosuspensions for drug delivery system and cytotoxicity evaluation in vitro. Advanced Fiber Materials. 2019; 1: 152-162.
26. Clement J, Rae A. Therapeutic drug combinations and delivery systems comprising c-raf kinase antisense polynucleotides for treating ocular diseases and disorders. Google Patents. 2007.
27. Guo CJ, Hou XY, Liu YH, Zhang YC, Xu HY, Zhao F, Chen DQ. Novel Chinese Angelica Polysaccharide Biomimetic Nanomedicine to Curcumin Delivery for Hepatocellular Carcinoma Treatment and Immunomodulatory Effect. Phytomedicine. 2021; 80: 153356.
28. Wang YF, Xiao J, Duan YC, Miao M, Huang B, Chen J, et al. Lycium barbarum Polysaccharide Ameliorates Sjögren's Syndrome in a Murine Model. Molecular Nutrition & Food Research. 2018; 65(11): 2001118.
29. Chen DQ, Lian SN, Sun JF, Liu ZL, Zhao F, Jiang YT, et al. Design of novel multifunctional targeting nano-carrier drug delivery system based on CD44 receptor and tumor microenvironment pH condition. Drug Delivery. 2016; 23(3): 798-803.
30. Spadea A, Rios de la Rosa JM, Tirella A, Ashford MB, Williams KJ, Stratford IJ, et al. Evaluating the efficiency of hyaluronic acid for tumor targeting via CD44. Molecular pharmaceutics. 2019; 16(6): 2481-2493.
31. Bousoik E, Qadri M, Elsaid KA. CD44 receptor mediates urate crystal phagocytosis by macrophages and regulates inflammation in a murine peritoneal model of acute gout. Scientific reports. 2020; 10(1): 5748.
32. Thorne RF, Wang Y, Zhang Y, Jing X, Zhang XD, De Bock CE, Oliveira CS. Evaluating nuclear translocation of surface receptors: recommendations arising from analysis of CD44. Histochemistry and cell biology. 2020; 153(2): 77-87.

33. Hou XY, Lin H, Zhou XD, Cheng ZT, Li Y, Liu X, et al. Novel dual ROS-sensitive and CD44 receptor targeting nanomicelles based on oligomeric hyaluronic acid for the efficient therapy of atherosclerosis. Carbohydrate polymers. 2020; 232: 115787.
34. Agrawal DC, Hou HY, Cheng TM. The Evaluation of Competency-Based Diagnosis System and Curriculum Improvement of Information Management. International Journal of Information and Communication Technology Education (IJICTE). 2021; 17: 87-102.
35. Wang KL, Guo CJ, Dong X, Yu YM, Wang BJ, Liu WH, Chen DQ. In vivo evaluation of reduction-responsive alendronate-hyaluronan-curcumin polymer-drug conjugates for targeted therapy of bone metastatic breast cancer. Molecular pharmaceutics. 2018; 15(7): 2764-2769.
36. Fan B, Kang L, Chen LQ, Sun P, Jin MJ, Wang QM, et al. Systemic siRNA delivery with a dual pH-responsive and tumor-targeted nanovector for inhibiting tumor growth and spontaneous metastasis in orthotopic murine model of breast carcinoma. Theranostics. 2017; 7(2): 357-376.
37. Xu CT, Chen G, Nie X, Wang LH, Ding SG, You YZ. Low generation PAMAM-based nanomicelles as ROS-responsive gene vectors with enhanced transfection efficacy and reduced cytotoxicity in vitro. New Journal of Chemistry. 2017; 41: 3273-3279.
38. Wang L, Wu S, Tang H, Meier H, Cao D. An efficient probe for sensing different concentration ranges of glutathione based on AIE-active Schiff base nanoaggregates with distinct reaction mechanism. Sensors and Actuators B: Chemical. 2018; 273: 1085-1090.
39. Li YN, Ward MJ, Richardson RM, G'Sell M, Ghuman AS. Endogenous activity modulates stimulus and circuit-specific neural tuning and predicts perceptual behavior. Nature communications. 2020; 11: 1-11.
40. Raza A, Rasheed T, Nabeel F, Hayat U, Bilal M, Iqbal H. Endogenous and exogenous stimuli-responsive drug delivery systems for programmed site-specific release. Molecules. 2019; 24: 1117.
41. Fan HY, Zhu ZL, Zhang WL, Yin YJ, Tang YL, Liang XH, et al. Light stimulus responsive nanomedicine in the treatment of oral squamous cell carcinoma. European journal of medicinal chemistry. 2020; 199: 112394.
42. Wu Y, Song ZY, Wang HJ, Han HY. Endogenous stimulus-powered antibiotic release from nanoreactors for a combination therapy of bacterial infections. Nature communications. 2019; 10(1): 4464.
43. Chen DQ, Sun KX, Mu HJ, Tang MT, Liang RC, Wang AP, et al. pH and temperature dual-sensitive liposome gel based on novel cleavable mPEG-Hz-CHEMS polymeric vaginal delivery system. International journal of nanomedicine. 2012; 7 2621-2630.
44. Chen DQ, Yu HY, Sun KX, Liu WH, Wang HB, Chen DQ, et al. Dual thermoresponsive and pH-responsive self-assembled micellar nanogel for anticancer drug delivery. Drug Delivery. 2014; 21(4): 258-264.
45. Fan JH, Zheng FJ, Li SY, Cui CT, Jiang S, Zhang J, et al. Hydrogen sulfide lowers hyperhomocysteinemia dependent on cystathionine γ lyase S-sulfhydration in ApoE-knockout atherosclerotic mice. British journal of pharmacology. 2019, 176: 3180-3192.

46. Wang J, Guo YW, Liu B, Jin XD, Liu LJ, Xu R, et al. Detection and analysis of reactive oxygen species (ROS) generated by nano-sized TiO2 powder under ultrasonic irradiation and application in sonocatalytic degradation of organic dyes. Ultrasonics Sonochemistry. 2011; 18(1): 177-183.
47. Ye M, Han Y, Tang J, Piao Y, Liu X, Zhou Z, Gao J, Rao J, Shen Y. A tumor-specific cascade amplification drug release nanoparticle for overcoming multidrug resistance in cancers. Advanced Materials. 2017; 29(38): 1702342.
48. Cheng R, Meng F, Deng C, Zhong Z. Bioresponsive polymeric nanotherapeutics for targeted cancer chemotherapy. Nano Today. 2015; 10: 656-670.

# Figures

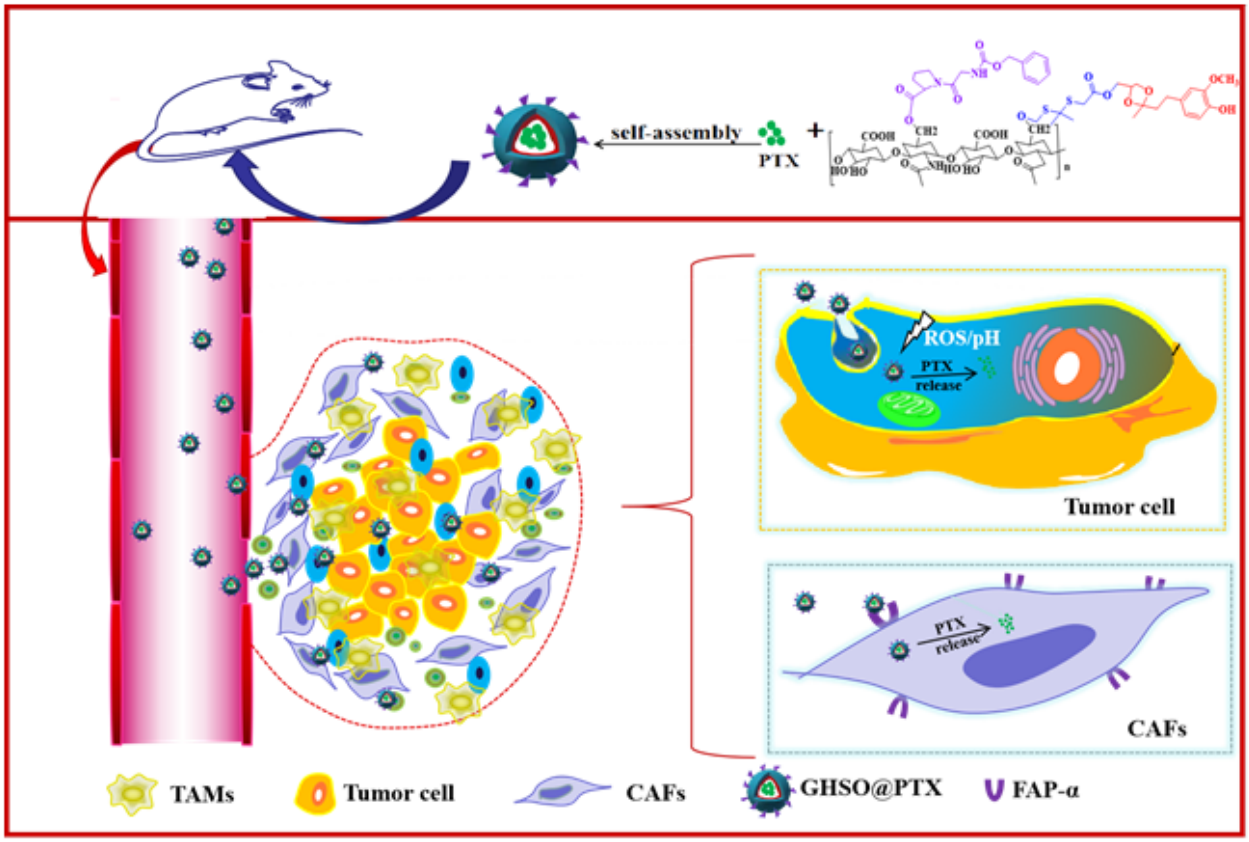


**Figure 1**

Schematic illustration of structure of GHSO@PTX

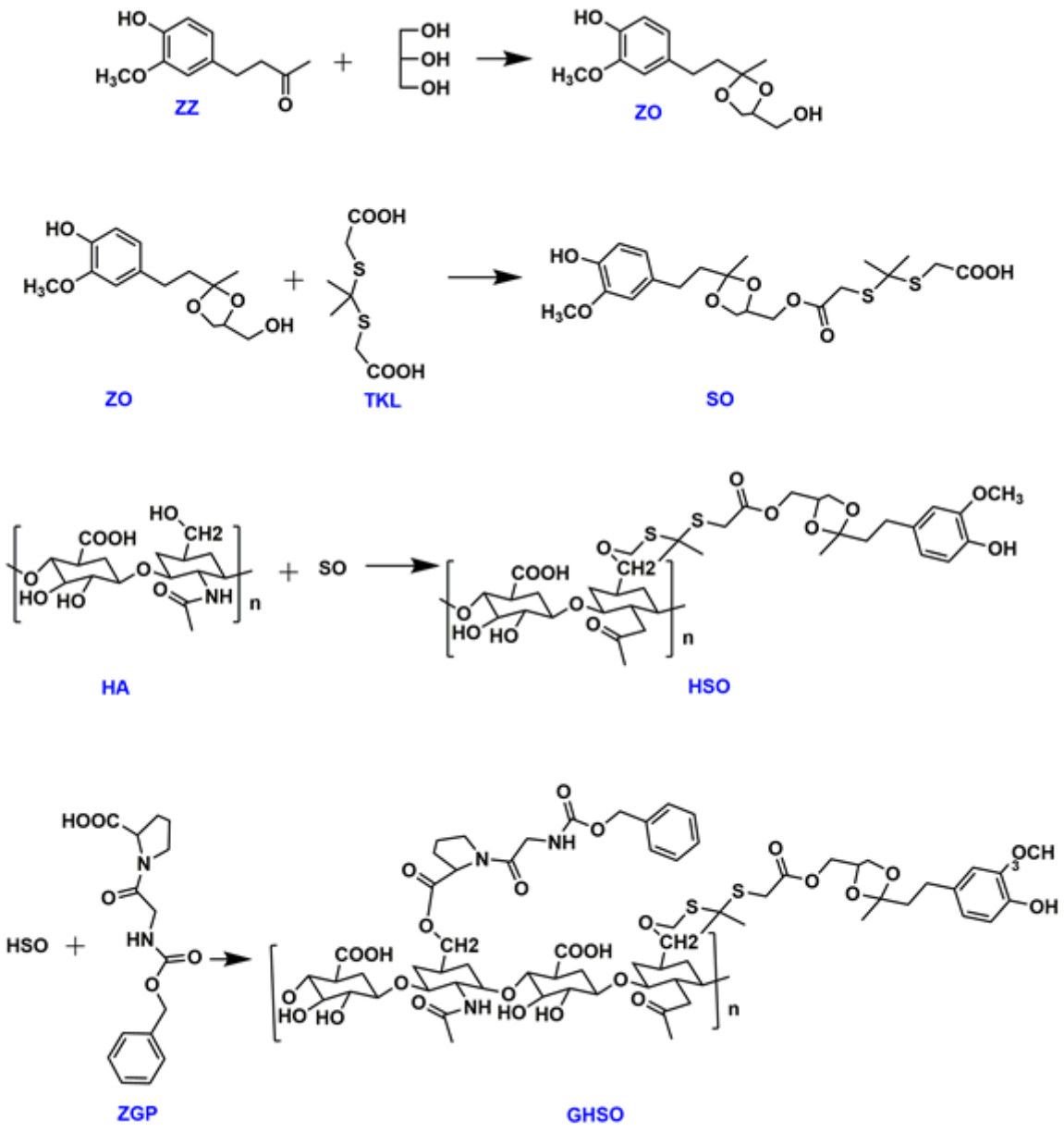


## Figure 2

Design route of GHSO

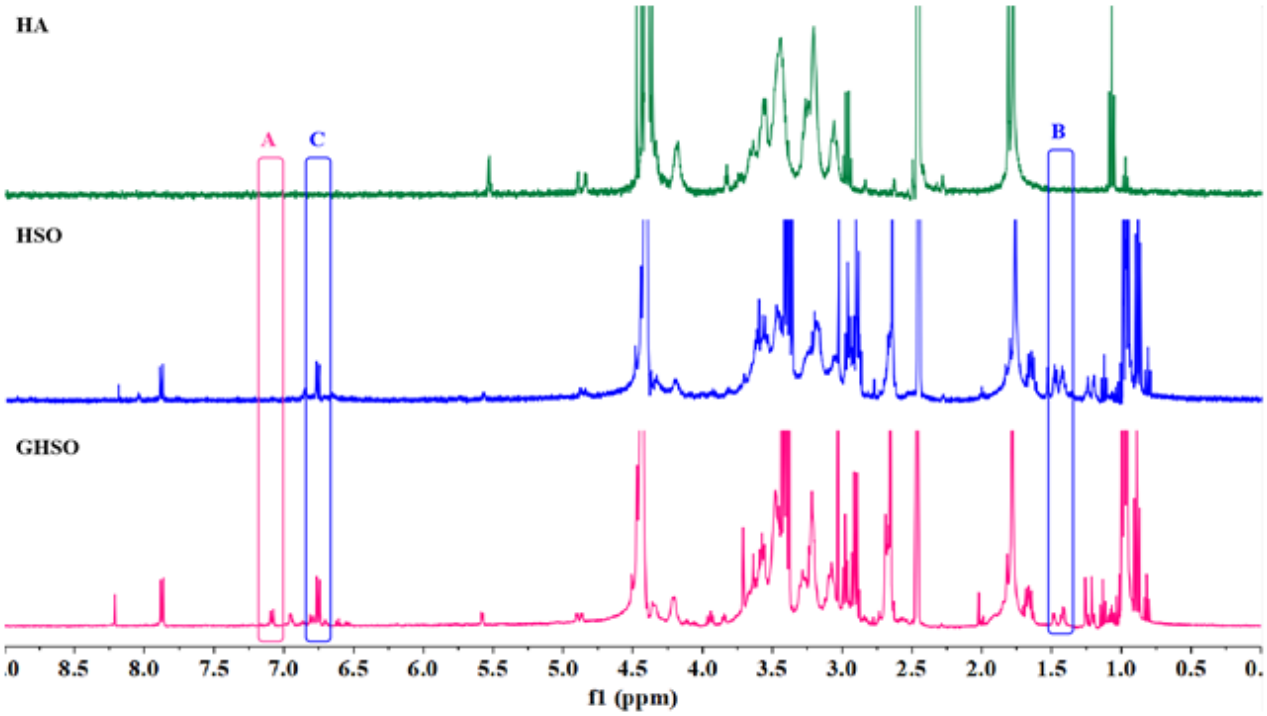


## Figure 3

The 1H-NMR spectra of HA、HSO and GHSO

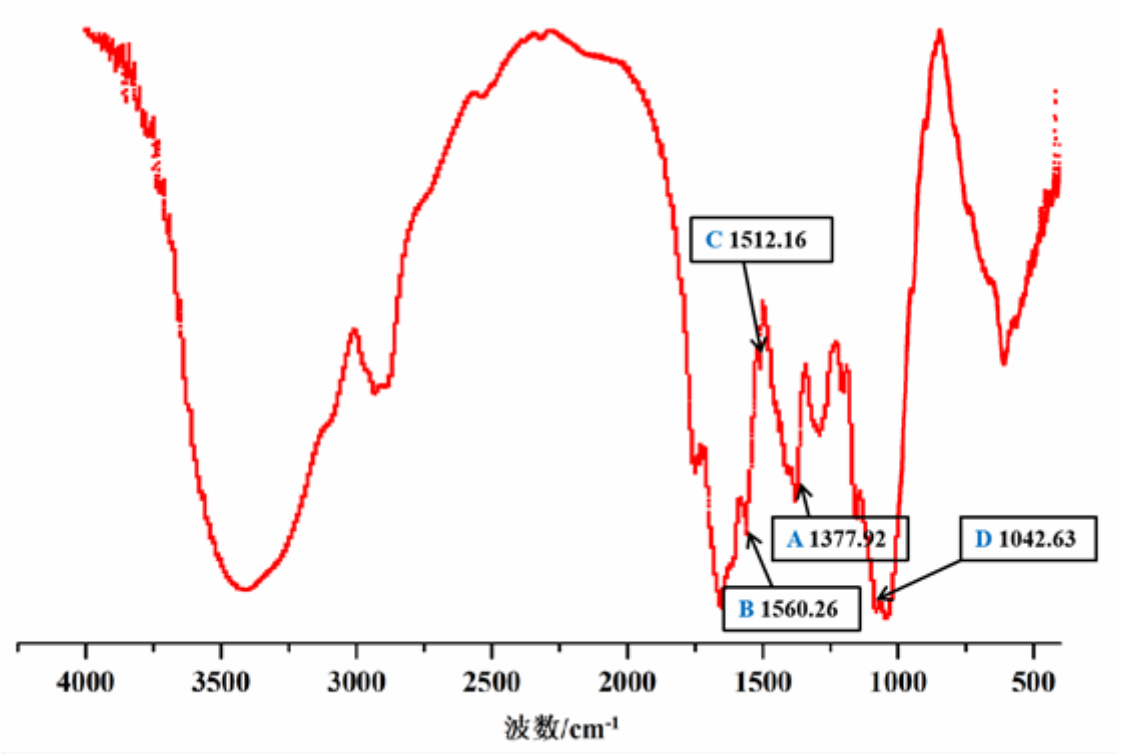


## Figure 4

The FT-IR spectra of GHSO

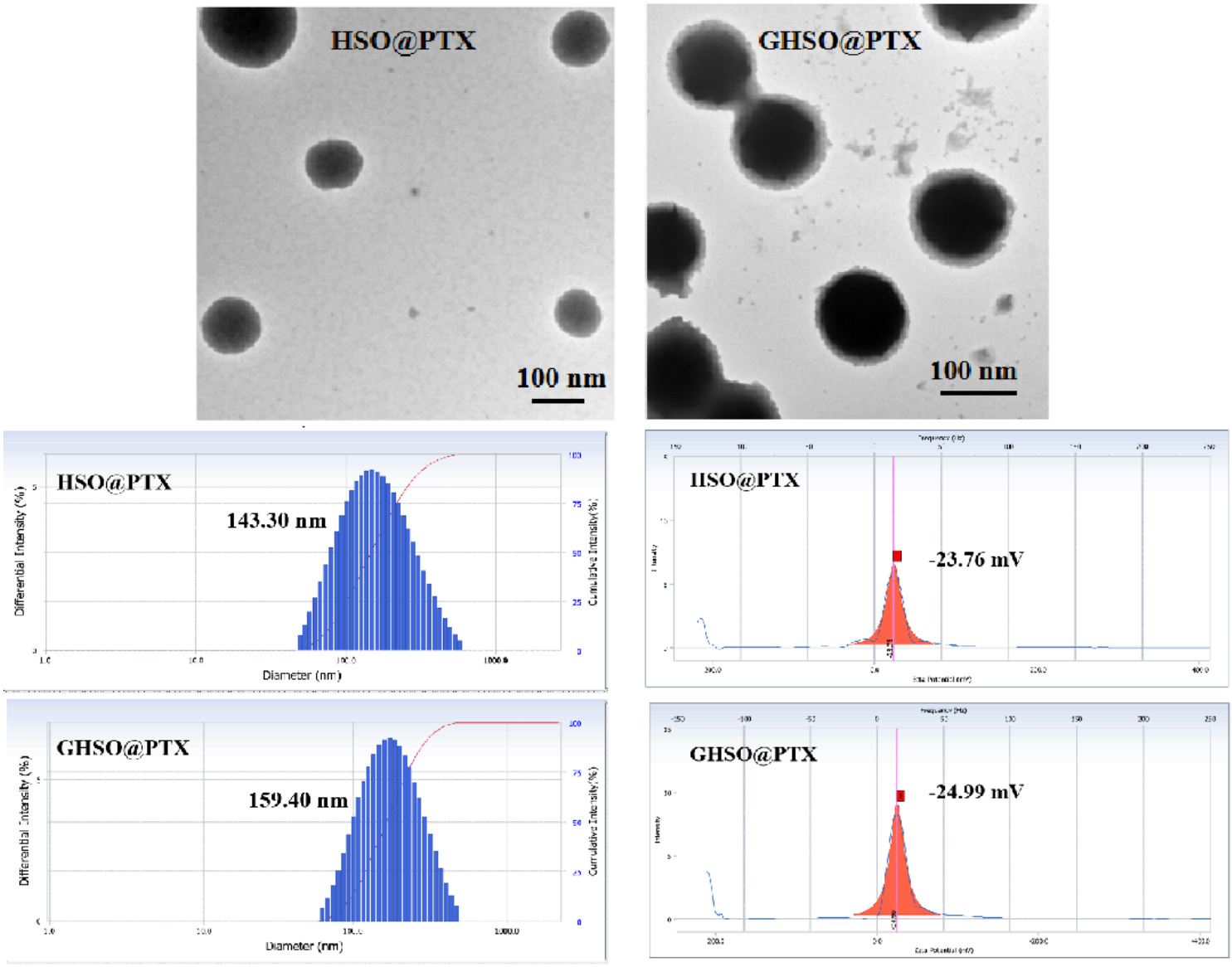


## Figure 5

The TEM morphology, size, zeta of HSO@PTX micelles and GHSO@PTX micelles

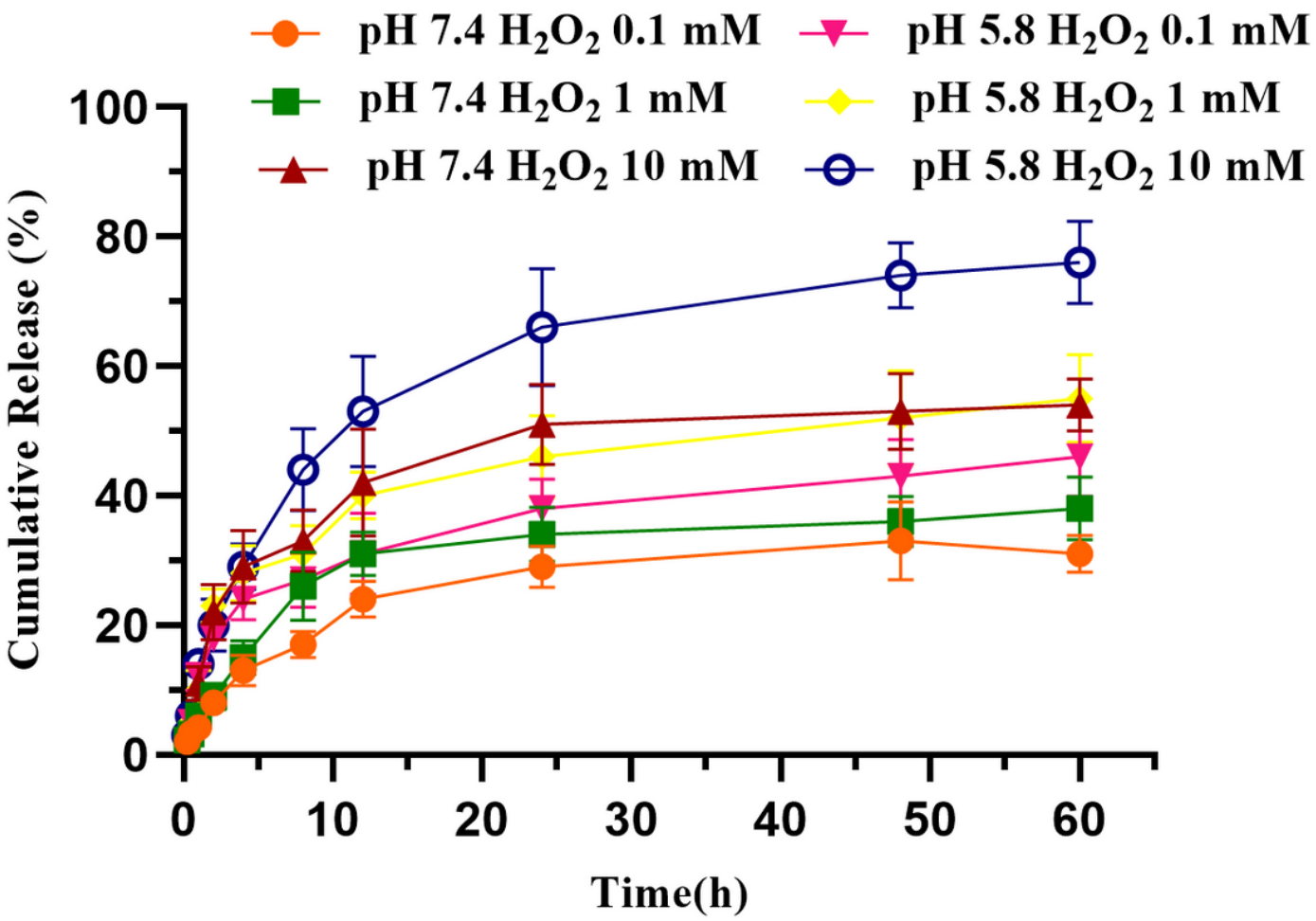


**Figure 6**

Curve of GHSO@PTX releasing PTX in different environments

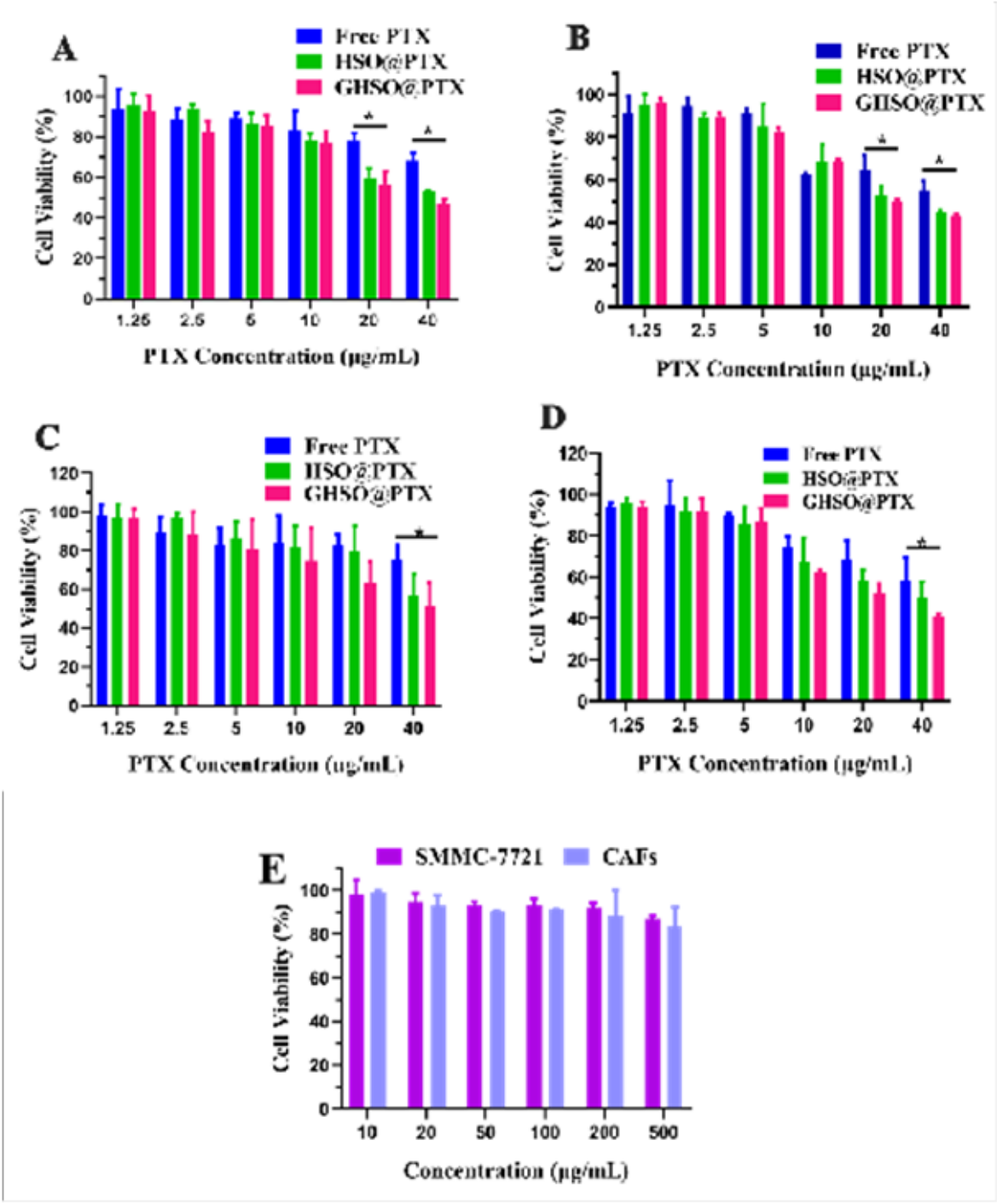


## Figure 7

The cytotoxicity of different formulations 24 h (A) and 48 h (B) to SMMC-7721 cells; the cytotoxicity of of different formulations 24 h (C) and 48(D) to CAFs cells; (E) The cytotoxicity of blank micelles to SMMC-7721 and CAFs cells. (*P<0.05)

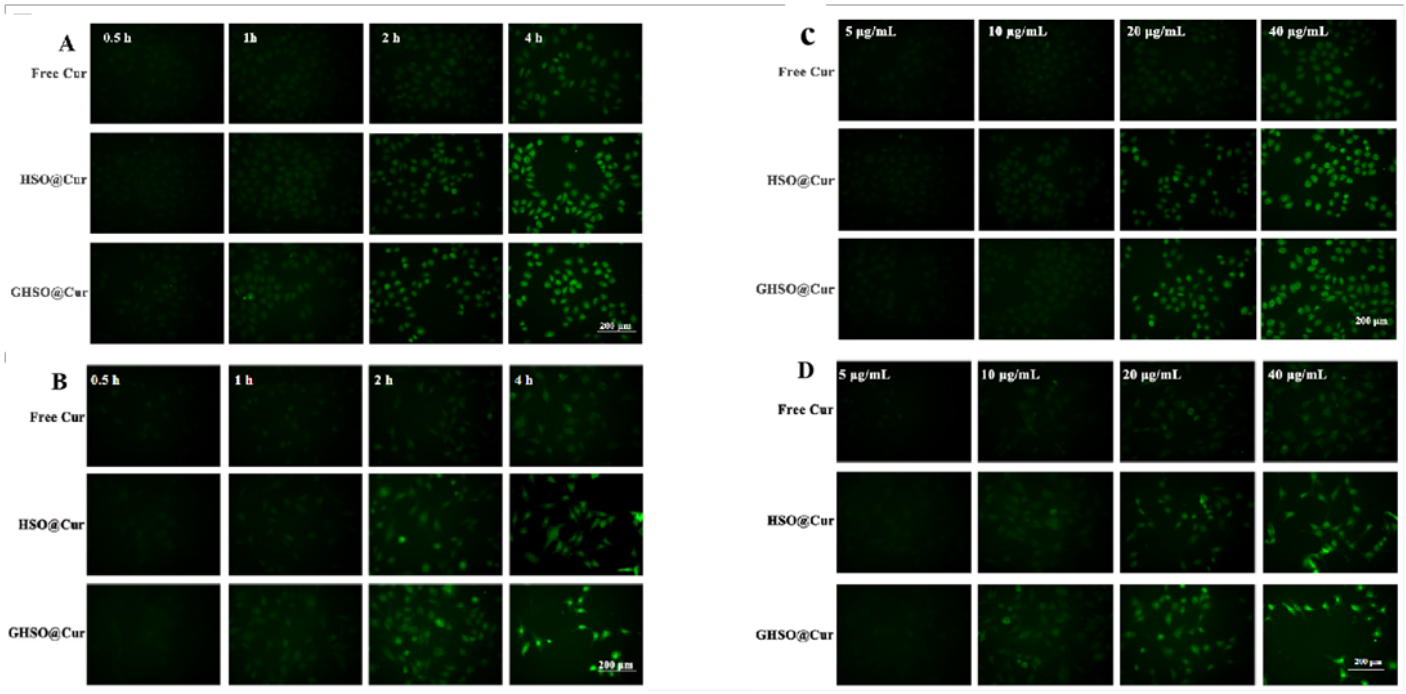


## Figure 8

The uptake of SMMC-7721 (A) and CAFs (B) after different administration times; The uptake of SMMC-7721 (C) and CAFs (D) after different administration concentration

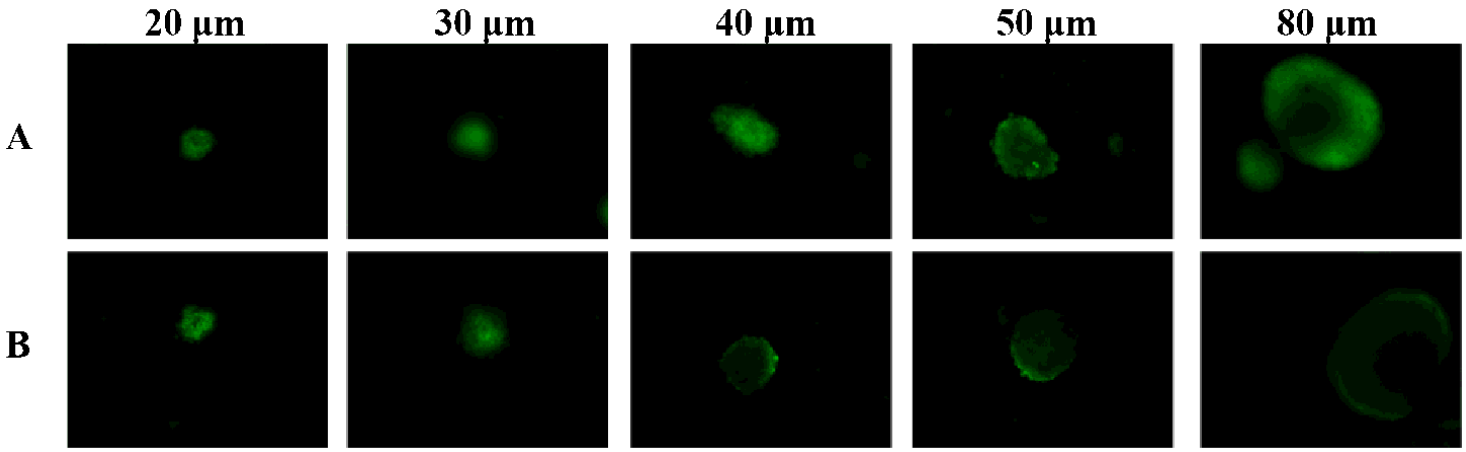


## Figure 9

The penetration of GHSO@Cur (A) and HSO@Cur (B) in 3D tumor sphere

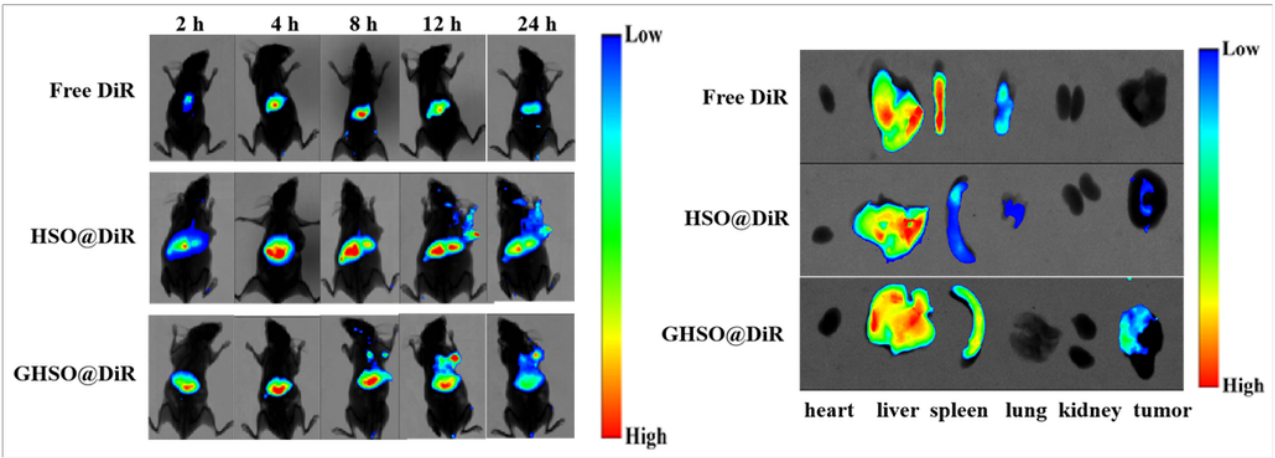


## Figure 10

The fluorescence of nude mice at different time intervals (2 h, 4 h, 8 h, 12 h and 24 h); The fluorescence intensity images of isolate organ and tumor tissues in nude mice.

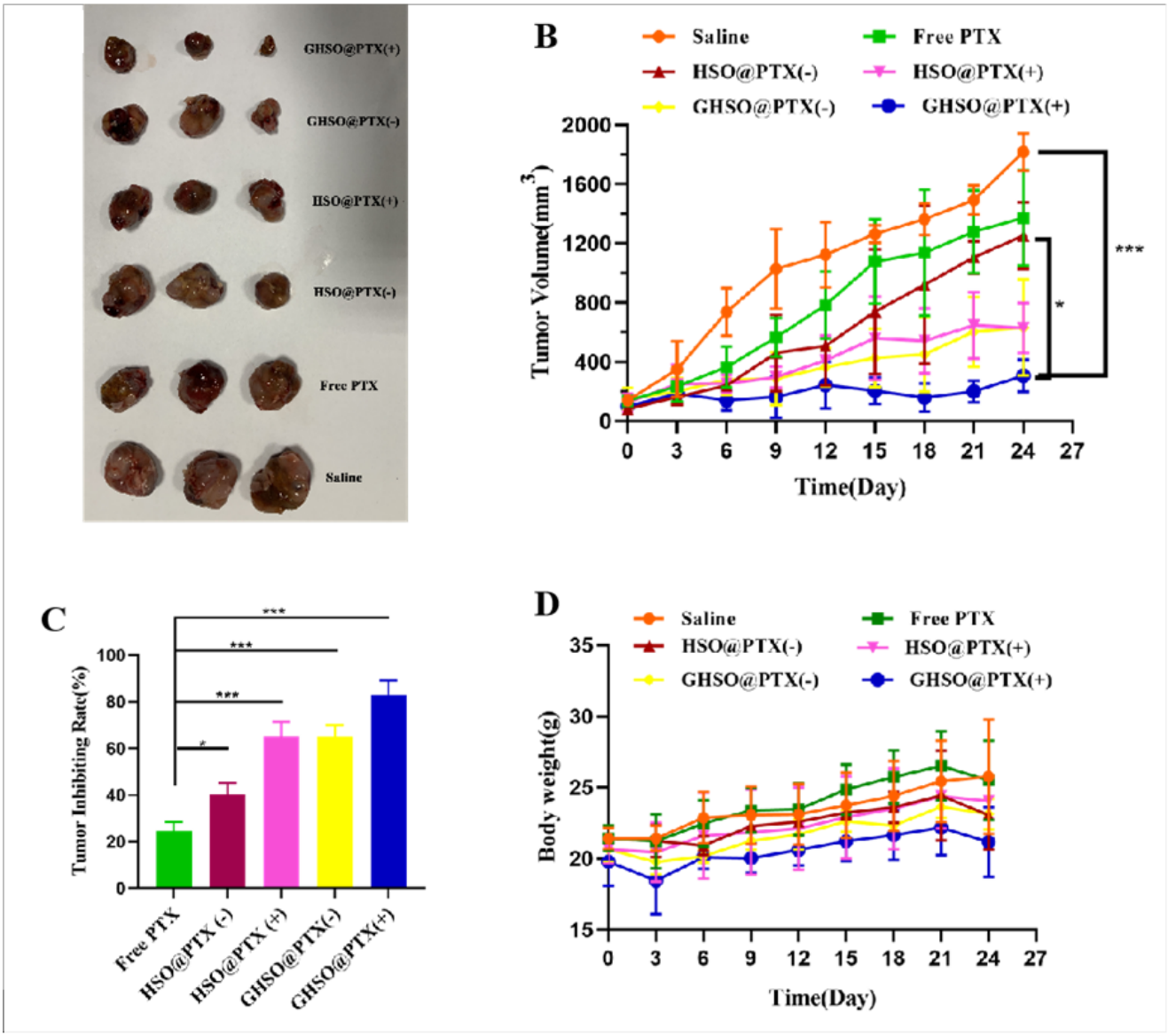


## Figure 11

(A) The photographs of tumors from different groups. (B) The tumor volume changes from different groups. (C) The tumor inhibition rate from different groups. (D) The body change of tumor-bearing nude mice. n=3; *P < 0.05, **P < 0.01.

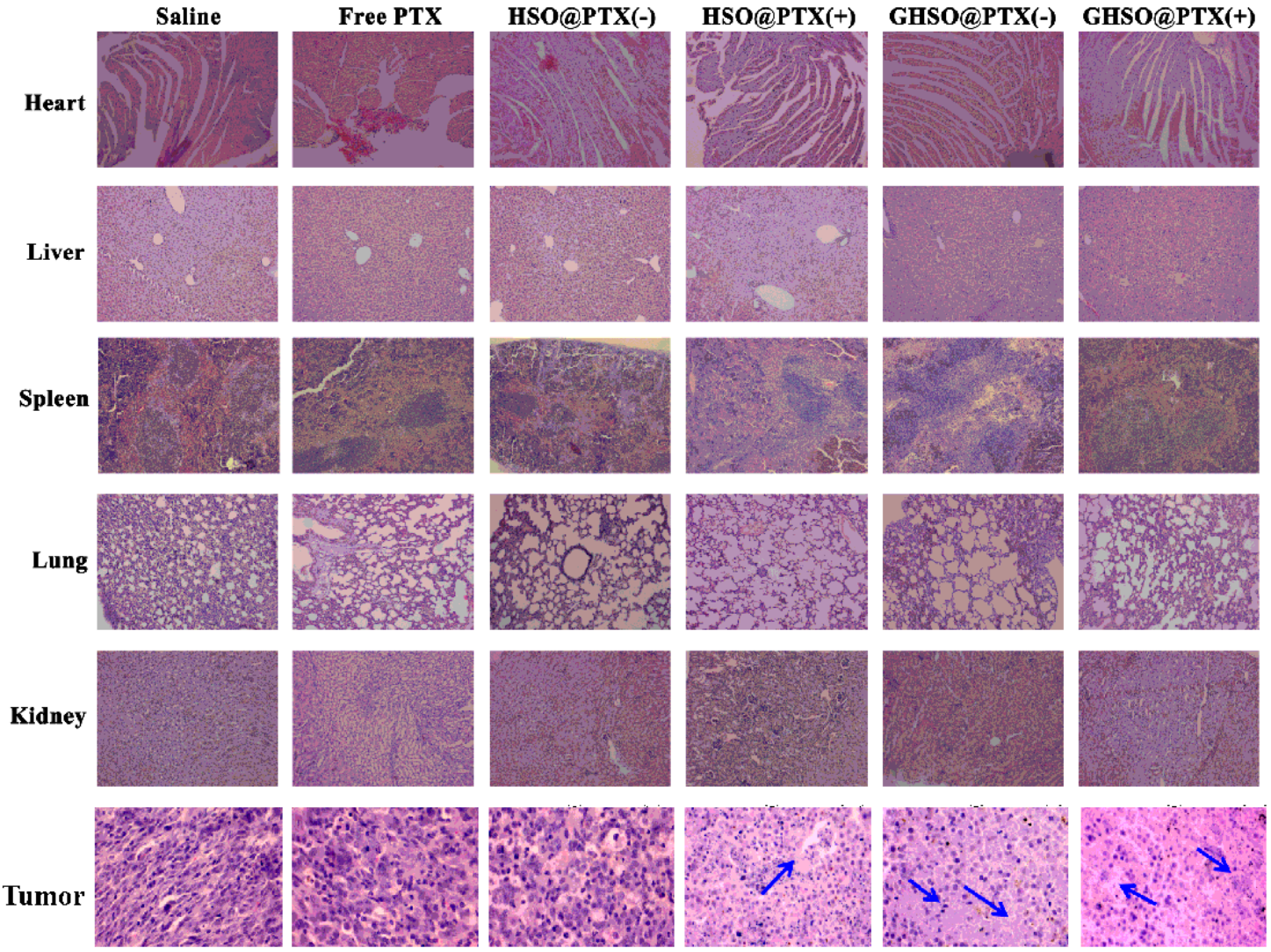


Figure 12

H&E staining of major organs and tumor issue in different administration groups

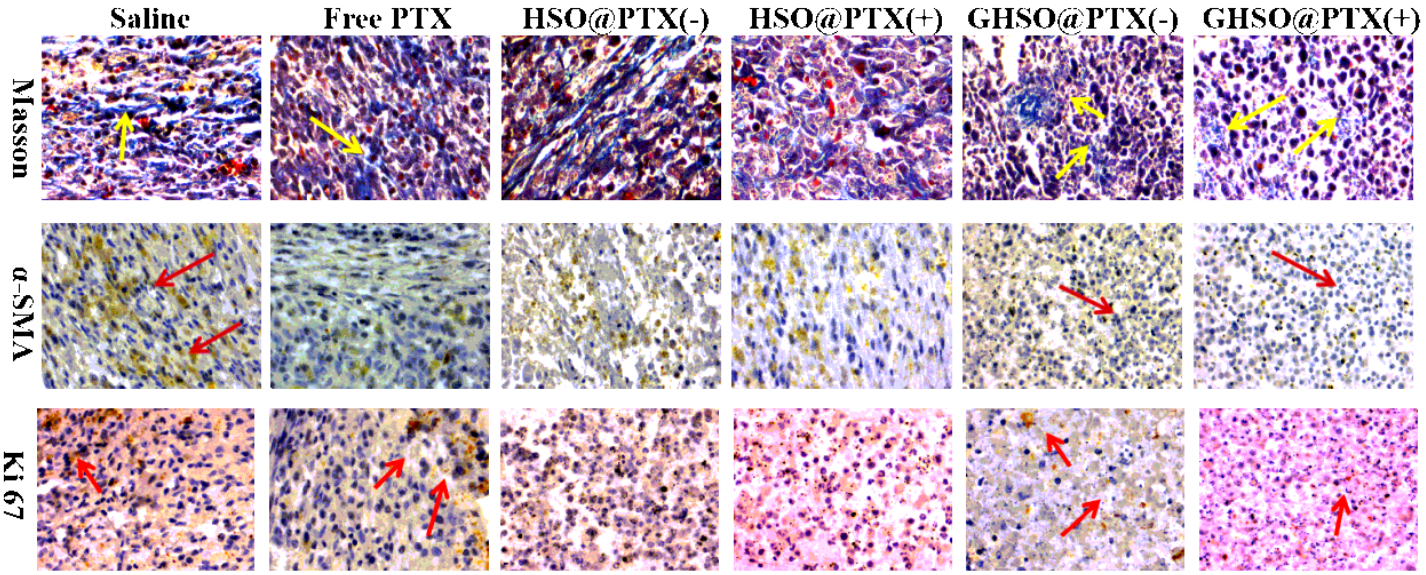

**Figure 13**

Masson staining, α-SMA staining and Ki 67 expression of tumor tissue.

## Supplementary Files

This is a list of supplementary files associated with this preprint. Click to download.

- GraphicalAbstract.doc